ZrO2 addition in soda-lime aluminoborosilicate glasses containing rare earths: Impact on rare earths environment and crystallization

Arnaud Quintas, Daniel Caurant, Odile Majérus, Pascal Loiseau, Thibault Charpentier, Jean-Luc Dussossoy

ZrO_2 addition in soda-lime aluminoborosilicate glasses containing rare earths : Impact on rare earths environment and crystallization

Arnaud Quintas [a], Daniel Caurant [b,*], Odile Majérus [b], Pascal Loiseau [b], Thibault Charpentier [c], Jean-Luc Dussossoy [d]

[a] *Laboratoire Commun Vitrification AREVA-CEA, 30207 Bagnols-sur-Cèze, France*

[b] *Chimie ParisTech, PSL Research University, CNRS, Institut de Recherche de Chimie Paris (IRCP), 75005 Paris, France*

[c] *NIMBE, CEA, CNRS, Université Paris-Saclay, CEA Saclay, 91191 Gif-sur-Yvette cedex, France*

[d] *CEA, DEN, DE2D/SEVT – Marcoule, F-30207 Bagnols sur Cèze, France*

Abstract

The effect of adding increasing ZrO_2 content on the environment of Nd^{3+} ions in a glass belonging to the SiO_2-B_2O_3-Al_2O_3-Na_2O-CaO system was investigated both by optical absorption spectroscopy and Nd-EXAFS (L_{III}-edge). In agreement with the evolution of the structure of the glassy network and more particularly of the distribution of Na^+ and Ca^{2+} ions with ZrO_2 addition put in evidence in a previous study, it is shown here that the average Nd-O distance continuously increases whereas the bond covalency decreases with zirconium content. This result can be explained both by the decrease of the amount of non-bridging oxygen atoms (NBOs) and by the increase of the proportion of Ca^{2+} ions acting as charge compensators in the neighborhood of neodymium polyhedra in the

[*] Corresponding author: E-mail address: daniel.caurant@chimie-paristech.fr (Daniel Caurant)

depolymerized regions of the glass structure. This evolution is due to a competition in favor of zirconium between Zr and Nd for Na^+ cations charge compensators. The local structural evolution around neodymium is probably responsible for the evolution of the crystallization tendency - increase of Nd-rich apatite ($Ca_2Nd_8(SiO_4)_6O_2$) crystallization in the bulk - observed in this work both during melt cooling and glass heating by increasing ZrO_2 content. It is proposed that the nucleating effect of ZrO_2 on apatite crystallization put in evidence here is mainly due to the changes that are indirectly induced by zirconium in the neighborhood of Nd^{3+} ions (destabilization) rather than to the formation of Zr-rich crystals that would then act as nucleating phase for apatite.

1. Introduction

ZrO_2 is frequently added in industrial glass compositions because of the special properties it imparts to these glasses. For instance, it is introduced in alkali-resistant glass fibers for reinforcement of cement products [1] and as nucleating agent in various glass-ceramics [2,3,4]. Zirconium is also abundant in the borosilicate glasses used to immobilize the nuclear wastes arising from the reprocessing of civil spent nuclear fuel [5]. In order to complete the numerous studies performed on borosilicate nuclear glasses to understand the role of ZrO_2 on their alteration mechanisms in water [6,7], the effect of ZrO_2 on their crystallization properties must be also investigated. Indeed, zirconium may be responsible for the appearance of crystalline phases during cooling of the melt [8,9,10,11]. For instance, Zr-containing phases such as $ZrSiO_4$ (zircon) and ZrO_2 (baddeleyite) may crystallize if the solubility limit is exceeded [12,13]. Moreover, because of its well-known role of nucleating agent in various silicate glasses [14,15,16], zirconium could also induce the crystallization of Zr-free phases.

Rare earths (RE) are frequently added in glasses for their optical properties but they are also abundant fission products (mainly from La to Sm) in nuclear waste solutions [5,17]. They are also frequently used in laboratories as non-radioactive actinide surrogates to prepare inactive glasses. Because of their high field strength, RE^{3+} ions may separate and crystallize as RE-rich phases - such as the silicate apatite phase $Ca_2RE_8(SiO_4)_6O_2$ - during glass preparation if their concentration is high in the melt. As such phases may incorporate in their structure a significant fraction of the minor actinides (Np, Am, Cm) present in the wastes due to their close chemical properties with RE, it is important to control their formation. As both ZrO_2 and RE_2O_3 are simultaneously present in nuclear waste glasses, the presence of high ZrO_2 content could increase the crystallization tendency of RE-rich phases during glass preparation. It thus appears important to investigate how the presence of increasing amount of zirconium could affect the local environment of RE^{3+} ions and their tendency to separate from the glass structure.

In the present study we have investigated the impact of adding increasing ZrO_2 concentration on the structure and the crystallization tendency of a Nd-rich soda-lime aluminoborosilicate glass that is a simplified version of a more complex glass developed to immobilize highly concentrated nuclear wastes, an aluminoborosilicate matrix under study and developed to immobilize highly concentrated nuclear wastes that would arise from the reprocessing of high burnup UO2 spent fuels [18] (Nd is the most abundant RE in fission products and is considered as a good minor actinide surrogate). In a recent companion paper [19], we focused our interest on the effect of the addition of ZrO_2 on the structure of the aluminoborosilicate glassy network and on the distribution of the modifier cations (Na^+, Ca^{2+}). In the present paper, a special attention has been paid to the evolution of the local environment of Nd^{3+} ions by using Nd-EXAFS and optical

absorption spectroscopy. This structural evolution has been then compared to that of the glass (network structure + distribution of charge compensators and modifier cations) obtained in [19] using a multi-spectroscopic approach. As indicated above, the glass crystallization tendency, especially the nature and the amount of crystalline phases induced by composition changes, is a topic of great interest for the waste form application. This has been examined and discussed in this paper in close relation with all structural investigation findings. In this work, different crystallization scenarios were imposed on the glass with increasing ZrO_2 content, among which a slow cooling of the melt in the crucible (1°C/min) that enables to assess the potential glass crystallization extent and a two-step isochronal heating above T_g (the glass transformation temperature) of quenched glass samples. This thermal stability study was aimed at understanding the role of Zr in crystallization processes and determining in which way ZrO_2 concentration should be adjusted to minimize crystallization occurrence. Several results of the present study were presented in a preliminary paper [20].

2. Experimental procedure

2.1. Glass synthesis

A glass series referred to as ZrxNd with ZrO_2 content varying from 0 to 5.69 mol% has been prepared for this study (Table 1). For all glasses, Nd_2O_3 concentration was close to 3.4 - 3.7 mol% (i.e. 15 - 16 wt%). Glasses were melted from the appropriate quantities of SiO_2, H_3BO_3, Al_2O_3, Na_2CO_3, $CaCO_3$, ZrO_2 and Nd_2O_3 reagent grade powders according to the procedure described in another paper [19]. Glass samples were annealed close to T_g for 2h to eliminate residual internal strains and to enable cutting thick plates for the need of optical absorption spectroscopy analysis. All samples were transparent and amorphous according to X-ray diffraction. The results of Inductively Coupled Plasma

Atomic Emission Spectrometry (ICP AES) given in Table 1 indicate only a relatively slight depletion in B_2O_3 (1 - 14 %) and Na_2O (4 - 6 %), these two oxides being the most volatile ones present in the melt. T_g was measured by differential thermal analysis (DTA) for all glasses of the ZrxNd series (Table 1). For this, about 200 mg of glass powders (particle size 80-125µm) were heated with a Netzsch STA409 apparatus in Pt crucibles using α-Al_2O_3 as reference material. The heating rate was maintained at 10°C/min until 1300°C. DTA was also used to follow the glass crystallization tendency with ZrO_2 addition (see Section 3.2).

2.2. Thermal treatment of glasses

The crystallization tendency of ZrxNd glasses was studied by two methods. The first method consists in a controlled cooling in air of the melt at 1°C/min from 1350°C to room temperature. 1-2 g of each glass was put in a Pt-Au (5 wt% Au) crucible - to avoid glass sticking on the crucible walls - heated at 6°C/min and melted during 30 min at 1350°C before controlled cooling. This method was intended for simulating the natural cooling of nuclear waste glass containers after casting (68°C/h in the bulk) and to study the crystallization process in representative industrial cooling conditions. It is important to note that this cooling scenario makes the amount of crystals formed in the glass highly sensitive to the surface state of the crucible because of the overriding role of surface crystallization process in these thermal conditions. As a result, considering the small quantities of glass samples used for this treatment (1 to 2 g), it is expected that, when crystal growth is strong, assessment of the pure bulk devitrification rate may be difficult. To better compare the effect of composition change on bulk crystallization characteristics and limit crucible influence which may additionally alter replicability of the experiment, a second heat treatment procedure was intended which aims to enhance bulk

crystallization to the detriment of surface crystallization. This second method is a two-step thermal treatment in air of nucleation (2h at T_g + 20°C) and growth (30h at the temperature T_p of the exothermic DTA peak of apatite crystallization between 930 and 977 °C, Table 1) in Pt–Au crucibles. For the two steps, samples of centimeter size were introduced directly and successively in two furnaces heated respectively at T_g + 20°C and T_p and were then quenched to room temperature after the second heating. The choice of the nucleation temperature slightly above T_g was done because the maximum of internal volume nucleation rate in glasses is known to frequently occur in this temperature range [21].

2.3. Characterization methods

The environment of Nd^{3+} ions in ZrxNd glasses was probed by Nd-EXAFS and optical absorption spectroscopy. X-ray absorption spectroscopy at the Nd L_{III}-edge (6212 eV) was carried out for Zr0Nd, Zr2Nd and Zr3Nd glasses at the synchrotron HASYLAB on the E4 beamline (Hamburg, Germany). Spectra were recorded in transmission mode at 77K in order to minimize thermal disorder. $Ca_2Nd_8(SiO_4)_6O_2$ and Nd_2SiO_7 ceramics prepared in our laboratory were also measured as references. Spectra simulation was performed according to the procedure described in [22], the signal corresponding to the first coordination shell was fitted in r-space supposing a single oxygen contribution and the mean Nd-O distance was extracted.

Nd^{3+} optical absorption spectra of ZrxNd glasses were recorded on a double CARY-5E spectrophotometer in transmission mode through polished plates of annealed glass of about 1 mm thickness. The temperature of the glass sample was maintained at 10K during spectra acquisition thanks to a He-cryostat so as to reduce the vibronic broadening and to simplify the spectra by increasing the population of the lowest Stark level of the $^4I_{9/2}$ ground state. Amongst the numerous transitions from the $^4I_{9/2}$ ground state to the $^{2S+1}L_J$

excited states of Nd^{3+} ions, the $^4I_{9/2} \rightarrow {}^2P_{1/2}$ transition at about 23200 cm^{-1} is of particular interest for structural investigation. With J = ½, the $^2P_{1/2}$ manifold is not split by the crystal field. Thus, when working at low temperature only the lowest Kramers doublet of the $^4I_{9/2}$ manifold is populated [22,23,24], this transition reflects the site distribution of Nd^{3+} ions in the glass and allows the monitoring of the manifold barycenters shift with the composition (nephelauxetic effect). Another interesting band on the optical absorption spectra of Nd^{3+} in glasses corresponds to the $^4I_{9/2} \rightarrow {}^4G_{5/2}, {}^2G_{7/2}$ transition which occurs at about 17250 cm^{-1} and is referred to as the hypersensitive band [24,25]. This band is hypersensitive because any variation in the crystal-field symmetry in neodymium environment is reflected by modifications of the overall intensity and shape of this double transition.

All heat treated samples were characterized by X-ray diffraction (XRD) and scanning electron microscopy (SEM). XRD was conducted with the help of a Siemens D5000 instrument using CoKα1 radiation (λ = 0.178897 nm). For this analysis, samples were crushed into powders with particle size < 80µm. Scanning electron microscopy (SEM) was completed with a HITACHI S2500 instrument equipped with a tungsten wire and operating at 15 kV. Heat-treated glass samples were set into resin studs which were polished and coated with a thin carbon layer.

3. Results and discussion

3.1. Evolution of neodymium environment

3.1.1. Structural role of RE^{3+} ions in peralkaline glasses

According to both spectroscopic results and molecular dynamic simulations reported in literature, RE oxides are known to act as modifier oxides in silicate glasses where they induce the formation of NBOs (Non-Bridging Oxygen atoms) in RE-O-Si

bonds with the silicate network [5,22,26,27]. For local charge compensation reasons and bond valence considerations, alkali and alkaline-earth cations are located near the RE-O-Si bonds and enable the solubilization of RE^{3+} ions in the silicate network. A schematic representation of the way RE^{3+} ions may enter into the structure of a peralkaline (Na_2O + CaO > Al_2O_3) soda-lime aluminoborosilicate glass has been presented in Fig. 18 of the companion paper [19]. It is proposed that RE^{3+}ions are preferentially located in depolymerized regions (DR) of the silicate network where they can find both NBOs to complete their coordination sphere [28,29,30,31] and alkali + alkaline-earth cations for local charge compensation.

3.1.2. Optical absorption

The environment of Nd^{3+} ions in the ZrxNd glass series was firstly investigated by optical absorption spectroscopy (Fig. 1). The evolution of the position of the $^4I_{9/2} \rightarrow {}^2P_{1/2}$ band is reported in Fig. 2 as a function of ZrO_2 content. A quite linear shift of the transition towards higher energy is observed. Consistently with other studies performed on Nd-bearing glasses [23,24,32], this high energy shift can be correlated to the increasing electron-electron Coulombic repulsion within the f valence shell of Nd^{3+} ions due to a decreasing covalency of the Nd-O bonds (nephelauxetic effect). Such a behavior was also observed in a previous work [23] performed on similar soda-lime aluminoborosilicate glass compositions (Ca/Na glass series) with 1.90 mol% ZrO_2 and 3.56 mol% Nd_2O_3 (these glass compositions are derived from that of Zr1Nd glass) but for which the ratio R = 100·[CaO]/([CaO] + [Na_2O]) varied from R = 0 ([CaO] = 0) to R = 50 ([Na_2O] = [CaO]) . For comparison with the results obtained for ZrxNd glasses, the data obtained in this previous work [23] are also reported in Fig. 2. A similar regular shift of the $^4I_{9/2} \rightarrow {}^2P_{1/2}$ band position towards higher energy was observed and was attributed

to a decrease of the proportion of Na^+ ions in favor of Ca^{2+} ions in the surrounding of Nd^{3+} ions. When the amount of ZrO_2 increases in the glasses of the ZrxLa series, the band position becomes closer to that in the glasses of the Ca/Na series with the highest R ratio (compare for instance the position of the band of Zr3Nd and R = 50 glasses in Figs. 2a and 3). This similar evolution with ZrO_2 content and R ratio suggests that the environment of Nd^{3+} ions becomes richer in calcium when the amount of ZrO_2 increases along the ZrxNd series. This is confirmed by the evolution of the shape of the $^4I_{9/2} \rightarrow {}^4G_{5/2}$, $^2G_{7/2}$ hypersensitive transition (Fig. 1b) that becomes more and more similar to that of the glass of the Ca/Na series with the highest CaO content (R = 50). A progressive disappearance of the shoulders initially present on the low-energy side of the two main bands of this transition is observed with increasing ZrO_2 content that suggests the presence of modifier cations with higher field strength (Ca^{2+} vs Na^+) in the vicinity of Nd^{3+} cations [25].

3.1.3. Nd-EXAFS

Further analysis were done on the ZrxNd glass series by Nd L_{III}-edge EXAFS spectroscopy, that confirmed the evolution of local Nd^{3+} environment with varying the ZrO_2 content. The magnitudes of the Fourier transform of the k^3-weighted chi(k) EXAFS functions are shown in Fig. 3 with the results of the fit corresponding to the coordination shell (O neighbors). The evolution of the mean Nd-O distance deduced from fitting procedure is reported in Fig. 4 at the same time as the data deduced from the EXAFS study of the Ca/Na series with varying R ratio [23]. The mean Nd-O distance in the ZrxNd glass series linearly increases with ZrO_2 addition which is consistent with the optical results presented in the previous paragraph indicating a weakening in Nd-O bond covalency. The comparison with the evolution of the Nd-O distance of the Ca/Na series

[23] is in accordance with a change in the proportion of Na^+ and Ca^{2+} ions (increase of the proportion of Ca^{2+} ions) in the immediate surroundings of Nd^{3+} ions. Indeed, in [23] the mean Nd-O distance variation was correlated with the evolution of the distribution of Na^+ and Ca^{2+} ions within the glasses.

3.1.4. Comparison with the evolution of the network structure

All these results concerning the environment of Nd^{3+} ions are consistent with the results presented in the companion paper [19] on the evolution of the glassy network structure that demonstrated the preferential charge compensation of $(ZrO_6)^{2-}$ entities with Na^+ ions and the decrease of NBOs amount in glasses of the ZrxNd series. Indeed, if we consider that Nd^{3+} ions are mainly located in Na^+, Ca^{2+} and NBOs-rich regions (i.e. in depolymerized regions (DR), see Fig. 18 in [19]) of glass structure, the addition of ZrO_2 in the composition is expected to drain mainly Na^+ ions and thus to induce a decrease of the Na^+/Ca^{2+} ratio in the environment of Nd^{3+} ions (indicated by arrows in Fig. 18 in [19]). This relative enrichment in Ca^{2+} ions thus raises the mean bond valence between the oxygen atoms of Nd-O-Si bonds and the charge compensating cations ($Na^+ + Ca^{2+}$) because Ca^{2+} cations are doubly charged. As a response, to avoid the overbonding of oxygen atoms connecting Nd and Si, the Nd-O mean distance adjusts itself (it increases as shown by EXAFS, Fig. 4).

3.2. Evolution of the glass crystallization tendency

The crystallization of glasses of the ZrxNd series has been studied during heating both by DTA (exothermic effects) and a two-step thermal treatment (nucleation during 2h at T_g + 20°C followed by heating during 30h at T_p) and during cooling of the melt (from 1350°C to room temperature at 1°C/min). The DTA curves from which have been

determined the T_g and T_p values (Table 1) for the different glasses are shown in Fig. 5. For all glasses an exothermic effect associated with the crystallization of the Nd calcium silicate apatite $Ca_2Nd_8(SiO_4)_6O_2$ is observed as verified by XRD and EDX. It appears that the introduction of ZrO_2 in glass composition leads to an increase of the intensity of this effect (compare the DTA curve of glass Zr0 with those of other glasses) which indicates that ZrO_2 increases the apatite crystallization tendency during heating. Moreover, by increasing the particle size of the Zr1Nd glass from 20µm to 800µm, a progressive shift from 865 to 960°C of T_p (not shown) is observed which indicates that for this glass the crystallization is controlled by surface nucleation. For the two-step heat treated Zr0Nd and Zr1Nd glasses, the pictures and SEM images shown in Fig. 6 demonstrate that apatite preferentially crystallizes from the glass surface which is in accordance with the DTA results of the Zr1Nd glass. When the ZrO_2 content increases (Zr2Nd and Zr3Nd glasses), an increasing tendency of the samples to nucleate in the bulk is observed (Fig. 6). These results clearly show that apatite nucleation rate in the bulk is enhanced when the zirconia content in glasses increases, which demonstrates a nucleating effect of ZrO_2 on apatite crystallization. For all the heat treated samples of the ZrxNd glass series, we verified by XRD that $Ca_2Nd_8(SiO_4)_6O_2$ was the only crystalline phase (Fig. 7). After controlled cooling from the melt, it appeared by XRD (not shown) that apatite was still the only crystalline phase formed. Moreover, it was observed that the Zr-free sample (Zr0Nd) exhibits the lowest crystallization tendency during melt cooling (Fig. 8), confirming the promoting effect of ZrO_2 on crystallization put in evidence during glass heating (Fig. 6). Nevertheless, for all compositions, during melt cooling the apatite crystals have nucleated at the surface of the samples (see inset in Fig. 8) which is a phenomenon that frequently occurs because nucleation in the bulk is not promoted at high temperature.

Several studies reported in literature pointed out the nucleating effect of ZrO_2 in alkaline-earth aluminosilicate glasses by promoting the crystallization of ZrO_2 nanoparticles from Zr-rich regions of the glass structure [14,33,34,35,36]. In these works, Zr surroundings were specific (coordination higher than six; edge sharing with the silicate network; existence of Zr-O-Zr bonds) and the easy rearrangement of the Zr local surroundings was assumed to lead to nano-ZrO_2 crystal precursor. Nevertheless, another recent work published by the same team [15] underlined the fact that Zr could also have a strong nucleating effect in 6-fold coordination in a Li_2O-bearing aluminosilicate glass whereas when Li_2O was totally replaced by Na_2O in the same glass composition, Zr (that remained in 6-fold coordination) had not nucleating effect. Using Zr-EXAFS results these authors proposed that it was mainly the distribution of Zr in the glassy network (existence of direct Zr-Zr polyhedral linkages) rather than the Zr coordination that was responsible for the nucleating effect of ZrO_2 in these glasses [15].

The Zr-EXAFS results presented in another paper [19] showed that Zr was located in almost symmetric octahedral sites in ZrxNd glasses (at least for x = 1 and 3) (Table 3 in [19]) and no Zr-O-Zr linkages were put in evidence. This last result was in accordance with the fact that for all glass compositions there was enough charge compensators - and even enough Na_2O - to compensate all the $(AlO_4)^-$, $(BO_4)^-$ and $(ZrO_6)^{2-}$ entities (Table 9 in [19]) and thus to maintain isolated 6-fold coordinated Zr (no need to share oxygen atoms). Moreover, studies (not shown here) performed by transmission electron microscopy (TEM) and XRD on the Zr3Nd sample (i.e. on the sample of the ZrxNd series with the highest ZrO_2 content) heat treated at 660°C during a long duration (94h) did not reveal any crystallization in the bulk. We thus propose that the nucleating effect of ZrO_2 in our glasses has a different origin than the one presented by Cormier et al. [15] in their glasses (formation of nano-ZrO_2 crystals than then act as nucleation centers in the

bulk for the main crystalline phase). In our case, we suggest that the addition of ZrO_2 would act indirectly on apatite crystallization by modifying the solubility of Nd^{3+} ions (i.e. by destabilizing them) in the supercooled melt and in the glass but without forming Zr-rich crystalline phase that would then act as nucleation center. As Nd^{3+} is the most abundant cationic species in $Ca_2Nd_8(SiO_4)_6O_2$ apatite crystals, the decrease of neodymium solubility would affect both their nucleation and growth rates. This destabilization of Nd^{3+} ions in the glassy network may be explained as follows. By increasing the ZrO_2 content, the formation of more and more $(ZrO_6)^{2-}$ units mobilizes increasing quantities of Na_2O (see the inset in Fig. 2 in [19]) and the amount of NBOs decreases. This mobilization thus induces a drop in the amount of NBOs and of Na^+ charge compensators available respectively to form Nd-O bonds and to compensate the negative charge of $(NdO_7)^{4-}$ polyhedra (assuming that Nd mainly occurs in 7-fold coordination and is preferentially bonded to NBOs, see Fig. 18 in [19]), in spite of the decrease of the proportion of $(BO_4)^-$ units that release Na^+ cations and oxygen anions but not enough to charge compensate all $(ZrO_6)^{2-}$ entities (see Fig. 13 in [19]). Consequently, the presence of increasing quantity of $(ZrO_6)^{2-}$ units would hinder the insertion of Nd^{3+} in the silicate network and would thus favor apatite crystallization. More quantitatively, the increasing crystallization tendency of ZrxNd glasses with ZrO_2 content can be put in evidence by comparing the evolution of the amount of oxide charge compensators (Na_2O + CaO) available for the incorporation of Nd^{3+} cations with the evolution of the total amount of oxide charge compensators really necessary to the incorporation of all Nd^{3+} cations (Fig. 9a and Table 2). The amount of charge compensators available corresponds to $[Na_2O]$ + [CaO] - $[Al_2O_3]$ - N4$[B_2O_3]$ - $[ZrO_2]$ (the N4 values obtained by ^{11}B NMR for the ZrxLa series - similar to the ZrxNd series but with La^{3+} ions (no paramagnetic) replacing Nd^{3+} ions (paramagnetic) - were used to calculate this amount [19]). The

amount of charge compensators needed for neodymium was calculated by assuming that all Nd^{3+} ions are well solubilized in the glassy network if they do not have to share NBOs, i.e. if they are isolated of each other. In this case, if we consider that they are surrounded by 7 NBOs giving $(NdO_7)^{4-}$ units, they need 4 positive charges for compensation (i.e 4 moles of Na_2O + CaO for one mole of Nd_2O_3). Fig. 9a clearly shows that the amount of available charge compensators is close to the amount necessary to well solubilize Nd^{3+} ions only for the composition Zr0Nd, but as soon as ZrO_2 is introduced in glass composition the gap increases between the two amounts and the tendency of Nd^{3+} ions to separate from the glassy network and to crystallize as apatite is thus expected to increase. According to Fig. 9a, the strongest destabilization of Nd^{3+} would occur for Zr2Nd and Zr3Nd glasses. This is in agreement with the increasing bulk crystallization for these two glasses (Fig. 6).

Additionally, we further propose that the modification in the nature of the charge compensators available for Nd^{3+} solubilisation also contributes to the crystallization enhancement of apatite. Indeed, in previous works we showed that apatite crystallization was directly related to variation in Nd^{3+} surrounding. In particular, it was demonstrated that apatite crystallization was favored when the Ca/Na ratio increased in Nd^{3+} environment [37]. Here, the increasing content of ZrO_2 in the glass induces a preferential mobilization of Na^+ cations for charge compensation of $(ZrO_6)^{2-}$ entities, resulting in a gradual depletion of sodium in the local neodymium environment (see Fig. 18 in [19]). Consistently with our previous results [37], the local relative calcium enrichment in Nd^{3+} surrounding (Fig. 9b, Table 2) induced by ZrO_2 addition, is thus also expected to promote apatite crystallization. It is interesting to indicate here that we also observed a strong nucleating effect on apatite crystallization of Al_2O_3 content in a glass composition close to that studied in this paper [38]. This result was also explained by an effect of the

negatively charged $(AlO_4)^-$ units on the distribution of Na^+ cations in glass structure and then indirectly on the stability of RE^{3+} cations.

3.3. Consequences of the evolution of crystallization tendency on application

Concerning the application as nuclear waste form of the glass composition studied in this paper, it appears that due to the relatively high content of RE_2O_3 (15-16 wt%), increasing ZrO_2 content should be carefully considered because of apatite crystallization during glass synthesis and more particularly during cooling of the melt. Indeed, as $Ca_2RE_8(SiO_4)_6O_2$ crystals are able to incorporate minor actinides in their structure by substituting partially RE [39], according to their minor actinides content, crystals may swell and become amorphous under α self-irradiation during disposal and storage and then potentially induce cracks in the glass in their surrounding depending on the particle size and distribution (the stresses induced by a spherical particle of radius R in the surrounding glassy matrix are proportional both to the swelling and to R^3) [40,41]. On the contrary, if the aim is to prepare apatite-based glass-ceramic waste forms with small apatite crystals that would incorporate efficiently minor actinides to benefit from a double containment barrier [42,43], ZrO_2 may appears as an efficient nucleating agent during heating of the parent glass.

4. Conclusions

In this paper, a strong effect of ZrO_2 addition on the local environment of Nd^{3+} ions (increase of Nd-O distance and decrease of Nd-O covalency as shown respectively by Nd-EXAFS and optical absorption spectroscopy) and on the crystallization tendency of the Nd calcium silicate apatite phase ($Ca_2Nd_8(SiO_4)_6O_2$) during melt cooling or glass heating was put in evidence in a Nd-bearing aluminoborosilicate glass. The results

presented here are complementary and in agreement with the ones related to the evolution of the aluminoborosilicate glassy network, the distribution of Na^+ and Ca^{2+} ions and the environment of Zr^{4+} ions given in another paper [19]. Indeed, the preferential charge compensation of $(ZrO_6)^{2-}$ octahedra by Na^+ ions shown in [19] that affects the local Ca^{2+}/Na^+ ratio in the depolymerized regions of the glass structure (see Fig. 18 in [19]), especially in the surroundings of Nd^{3+} ions (need for charge compensation of $(NdO_7)^{4-}$ polyhedra) and the decrease in the amount of NBOs available to surround these ions (NBOs being also needed by zirconium to satisfy its 6-fold coordination) were both expected to seriously hinder the incorporation of neodymium in glass structure. The resulting destabilization of Nd^{3+} ions by adding increasing ZrO_2 amounts can thus explain the greater crystallization tendency of $Ca_2Nd_8(SiO_4)_6O_2$ apatite put in evidence in the present study. Promoting bulk crystallization, the well-known nucleating effect of ZrO_2 in glasses is thus confirmed for the composition studied here, but a different crystallization pathway than classically envisaged is proposed in the present case (lack of formation of small Zr-rich crystals than would then promote the crystallization of the main phase), consisting in an indirect effect of the incorporation of Zr^{4+} ions in glass structure that favorably competes against RE^{3+} for charge compensators (mainly Na^+) and NBOs.

Acknowledgments

The authors thank the CEA and the AREVA Chaire with Chimie-ParisTech and ENSTA-ParisTech for their contribution to the financial support of this study. We would also like to acknowledge the members of the HASYLAB synchrotron source (E4 beamline, Hamburg, Germany) for their help and availability during respectively the Nd L_{III}-edge EXAFS experiments. P. Vermaut (Chimie-ParisTech, France) is gratefully

acknowledged for the characterization of several samples by transmission electron microscopy (TEM).

Glass (mol%)	SiO_2	B_2O_3	Al_2O_3	Na_2O	CaO	ZrO_2	Nd_2O_3	T_g(°C)	T_p(°C)
Zr0Nd[a]	63.00	9.12	3.11	14.69	6.45	0	3.63		
Zr0Nd[b]	64.15	8.13	3.27	14.06	6.74	0	3.66	602	930
Zr1Nd[a]	61.81	8.94	3.05	14.41	6.33	1.90	3.56		
Zr1Nd[b]	60.39	8.56	3.31	14.93	7.04	2.04	3.73	611	934
Zr2Nd[a]	60.61	8.77	2.99	14.14	6.20	3.79	3.49		
Zr2Nd[b]	60.41	8.51	3.20	13.63	6.45	4.19	3.62	632	955
Zr3Nd[a]	59.42	8.60	2.94	13.86	6.08	5.69	3.42		
Zr3Nd[b]	58.41	8.51	3.15	13.65	6.48	6.24	3.56	642	977

Table 1. ([a]) Theoretical composition of ZrxNd glasses. ([b]) Analysed compositions of all ZrxNd glasses by ICP AES are also given for comparison. Increasing amount of ZrO_2 was added to Zr0Nd glass at the expense of all other oxides. The glass transformation temperature T_g (uncertainty +/- 3°C) and the temperature T_p of the exothermic peak associated with apatite crystallization of ZrxNd glasses determined by DTA (Fig. 5) are given in the two last columns.

Glass	$[Na_2O]_{av}$	[CaO]	$[Na_2O]_{av}$ + [CaO]	$4.[Nd_2O_3]$	$100.[CaO]/([Na_2O]_{av}+[CaO])$
Zr0Nd	7.01	6.74	13.75	14.64	49.02
Zr1Nd	6.02	7.04	13.06	14.92	53.90
Zr2Nd	3.09	6.45	9.54	14.48	67.61
Zr3Nd	1.78	6.48	8.26	14.24	78.45

Table 2. Evolution in ZrxNd glasses of the concentrations: $[Na_2O]_{av}$ of Na_2O available for the charge compensation of Nd^{3+} cations assuming that all $(AlO_4)^-$, $(BO_4)^-$ and $(ZrO_6)^{2-}$ units are only compensated by Na^+ cations; [CaO] of CaO available for the charge compensation of Nd^{3+} cations; $[Na_2O]_{av}$ + [CaO] of all charge compensators available for the charge compensation of Nd^{3+} cations; $4.[Nd_2O_3]$ of charge compensators needed to incorporate all Nd^{3+} cations as $(NdO_7)^{4-}$ entities. The last column indicates the percentage of Ca^{2+} cations available for the charge compensation of Nd^{3+} cations among the total amount of available charge compensators.

Figures captions

Fig. 1. (a) Evolution of the $^4I_{9/2} \rightarrow {}^2P_{1/2}$ optical absorption band of neodymium in glasses of the ZrxNd series (T = 10 K). The spectrum of the glass sample with R = 50 ([Na_2O] = [CaO]) studied in a previous work (Ca/Na series) [23] is also reported in the figure for comparison. (b) Evolution of the $^4I_{9/2} \rightarrow {}^4G_{5/2}$, $^4G_{7/2}$ hypersensitive optical absorption band of neodymium in glasses of the ZrxNd series (T = 10 K). * Shoulders on the low-energy side of the two main bands.

Fig. 2. (a) Evolution with zirconia content of the position of the $^4I_{9/2} \rightarrow {}^2P_{1/2}$ optical absorption band of Nd^{3+} ions in ZrxNd glasses. (b) Evolution of the position of the $^4I_{9/2} \rightarrow {}^2P_{1/2}$ absorption band of Nd^{3+} ions in glasses derived from the Zr1Nd glass by varying R = 100·[CaO]/([CaO]+[Na_2O]) from R = 0 ([CaO] = 0) to R = 50 ([Na_2O] = [CaO]) (Ca/Na series) [23]. (T = 10K)

Fig. 3. Magnitude of the Fourier transforms of the k^3chi(k) Nd L_{III}-edge EXAFS functions extracted from the XAS spectra (T = 77K) for ZrxNd glass series and oxygen shell fits (dots).

Fig. 4. (a) Evolution with zirconia content of the mean Nd-O distance in glasses of the ZrxNd series deduced from Nd L_{III}-edge EXAFS results shown in Fig. 3 (T = 77K) (b) Evolution of the mean Nd-O distance in glasses derived from the Zr1Nd glass by varying R = 100·[CaO]/([CaO]+[Na_2O]) from R = 0 ([CaO] = 0) to R = 50 ([Na_2O] = [CaO]) (Ca/Na series) [23]. (T = 6K)

Fig. 5. DTA curves of glasses of the ZrxNd series (particle size 80-125µm, heating rate 10°C/min). The exothermic effect (maximum at T_p) above 900°C is due to apatite crystallization for all the samples whereas the endothermic effect between 600 and 650°C is due to glass transformation. T_g and T_p values are given in Table 1.

Fig. 6. Pictures (top) and back-scattered electron microscopy images (bottom) of the samples of the ZrxNd series after the nucleation (2h at T_g + 20°C) + growth thermal treatment (30h at T_p). The purple coloration of the pictures is due to the presence of neodymium.

Fig. 7. XRD patterns of the samples of the ZrxNd series after the nucleation (2h at T_g + 20°C) + growth thermal treatment (30h at T_p). All the lines are due to apatite $Ca_2Nd_8(SiO_4)_6O_2$ crystals.

Fig. 8. Pictures (inset) and back-scattered electron microscopy images of the Zr0Nd and Zr1Nd samples after controlled cooling (1°C/min) from the melt (1350°C) to room temperature.

Fig. 9. (a) Evolution with ZrO_2 content of: (○) the total amount of charge compensators ($[Na_2O]_{av}$ + [CaO]) available to compensate all Nd^{3+} cations - and thus to facilitate their incorporation in the glassy network - assuming that $(AlO_4)^-$, $(BO_4)^-$ and $(ZrO_6)^{2-}$ units are only charge compensated by Na^+ cations ($[Na_2O]_{av}$ = $[Na_2O]$ - $[Al_2O_3]$ - N4$[B_2O_3]$ - $[ZrO_2]$, where N4$[B_2O_3]$ is the amount of B_2O_3 that forms BO_4 units). (●) the amount of charge compensators needed to enable the incorporation of all neodymimium as isolated Nd^{3+} cations 7-fold coordinated to NBOs ($(NdO_7)^{4-}$ polyhedra) and charge compensated

by 4 positive charges. (b) Evolution of the proportion of CaO among the charge compensators available to compensate all Nd^{3+} cations by considering that Na^{+} cations are preferentially used to compensate $(BO_4)^{-}$, $(AlO_4)^{-}$ and $(ZrO_6)^{2-}$ entities.

Figure 1

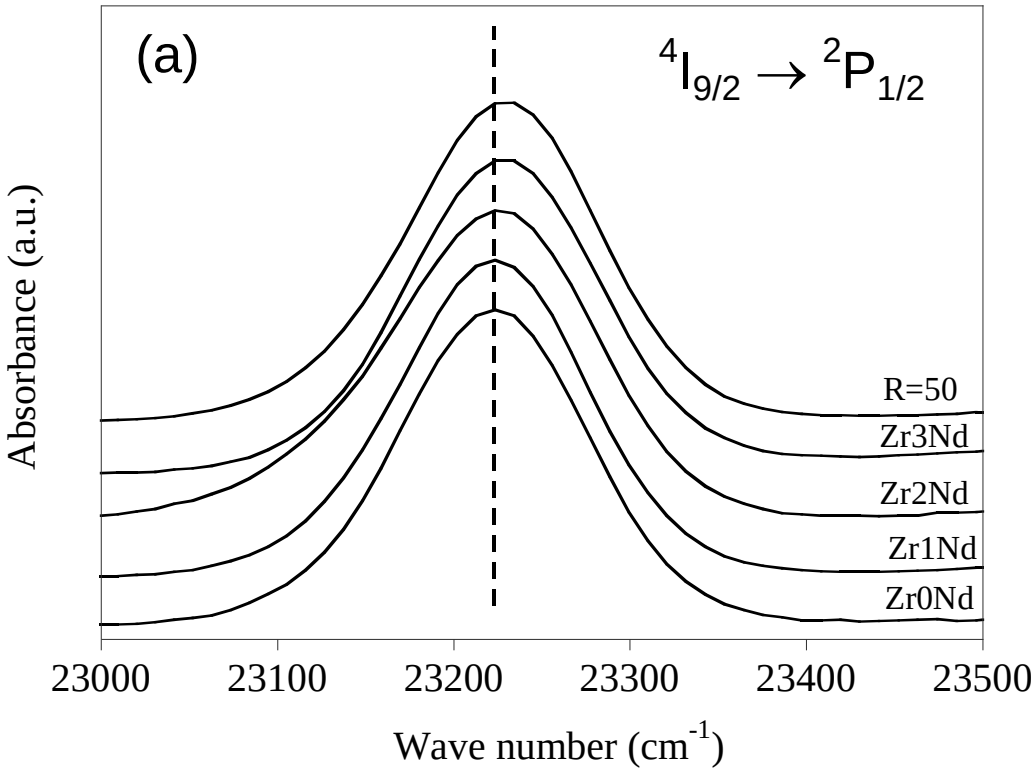
(a)
$^4I_{9/2} \rightarrow {}^2P_{1/2}$
Absorbance (a.u.)
R=50
Zr3Nd
Zr2Nd
Zr1Nd
Zr0Nd
23000
23100
23200
23300
23400
23500
Wave number (cm^{-1})

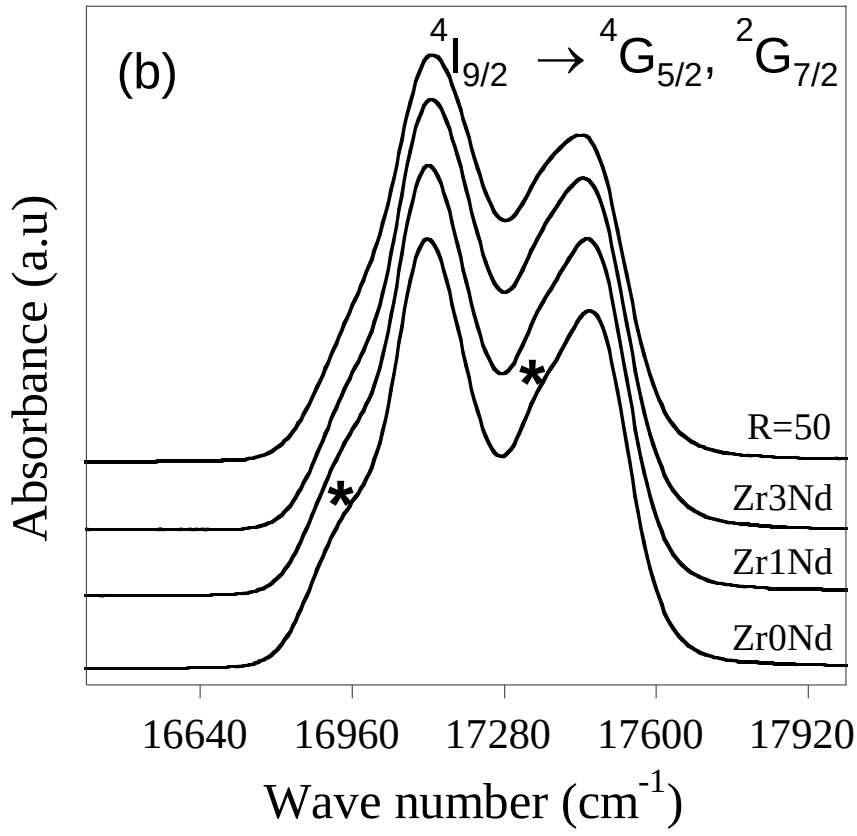
(b)
$^4I_{9/2} \rightarrow {}^4G_{5/2}, {}^2G_{7/2}$
Absorbance (a.u)
*
*
R=50
Zr3Nd
Zr1Nd
Zr0Nd
16640
16960
17280
17600
17920
Wave number (cm^{-1})

Figure 2

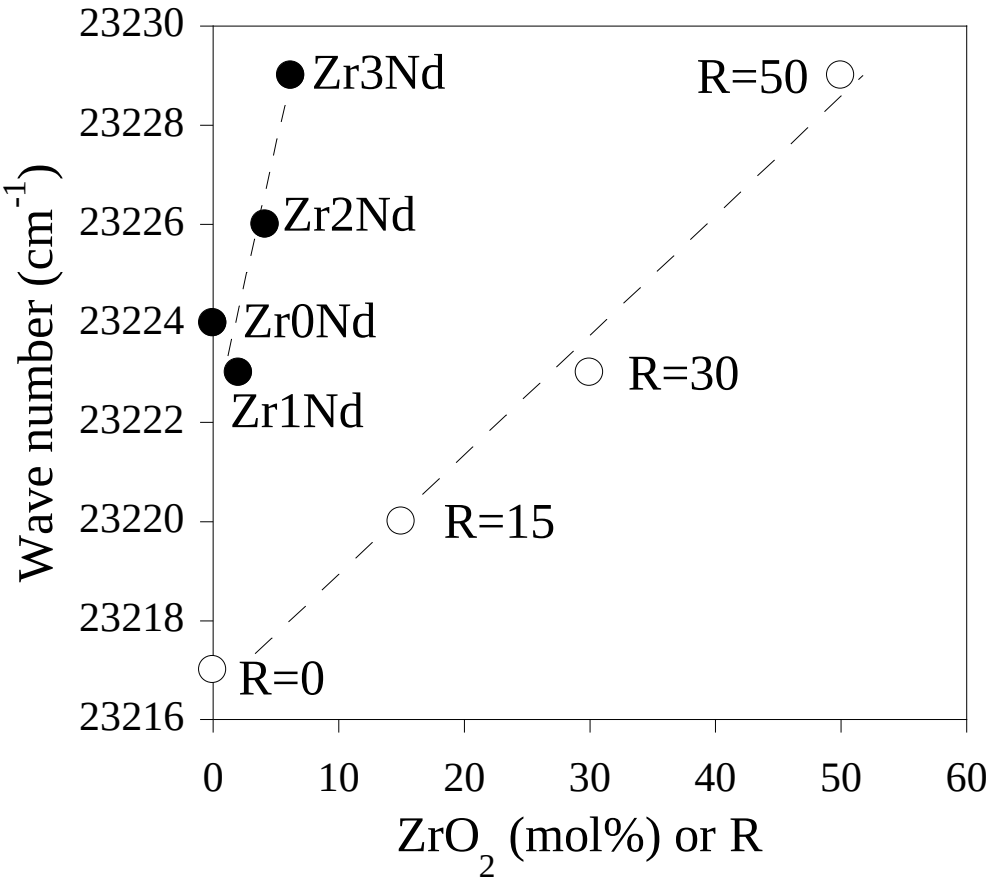
23230
23228
23226
23224
23222
23220
23218
23216
Wave number (cm-1)
Zr3Nd
Zr2Nd
Zr0Nd
Zr1Nd
R=50
R=30
R=15
R=0
0
10
20
30
40
50
60
ZrO2 (mol%) or R

Figure 3

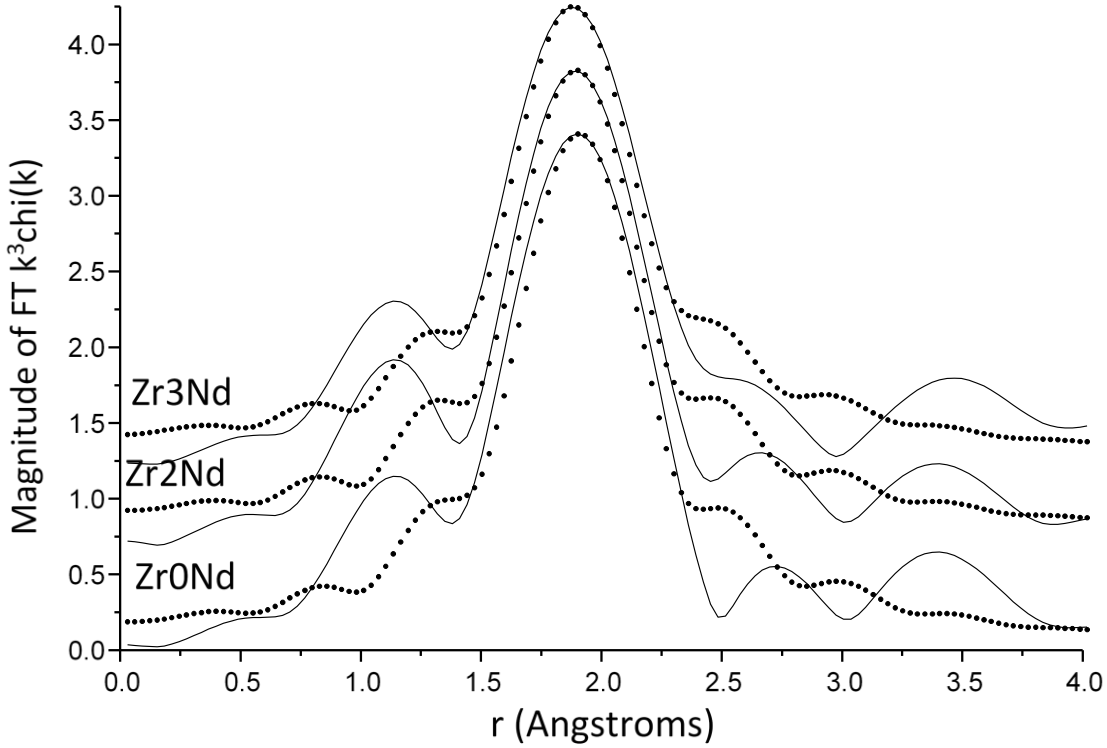
Magnitude of FT k3chi(k)
r (Angstroms)
Zr3Nd
Zr2Nd
Zr0Nd
0.0
0.5
1.0
1.5
2.0
2.5
3.0
3.5
4.0

Figure 4

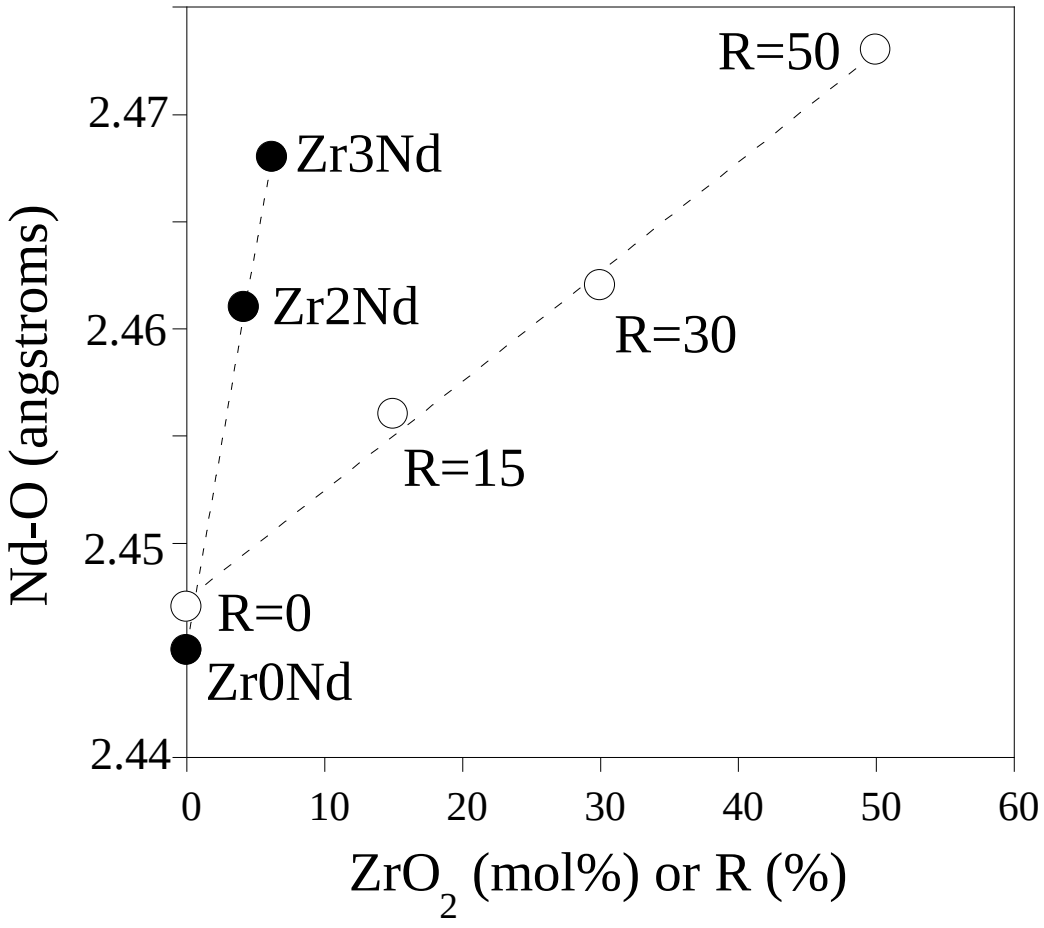
R=50
2.47
Zr3Nd
Zr2Nd
2.46
R=30
R=15
2.45
R=0
Zr0Nd
2.44
Nd-O (angstroms)
0
10
20
30
40
50
60
ZrO2 (mol%) or R (%)

Figure 5

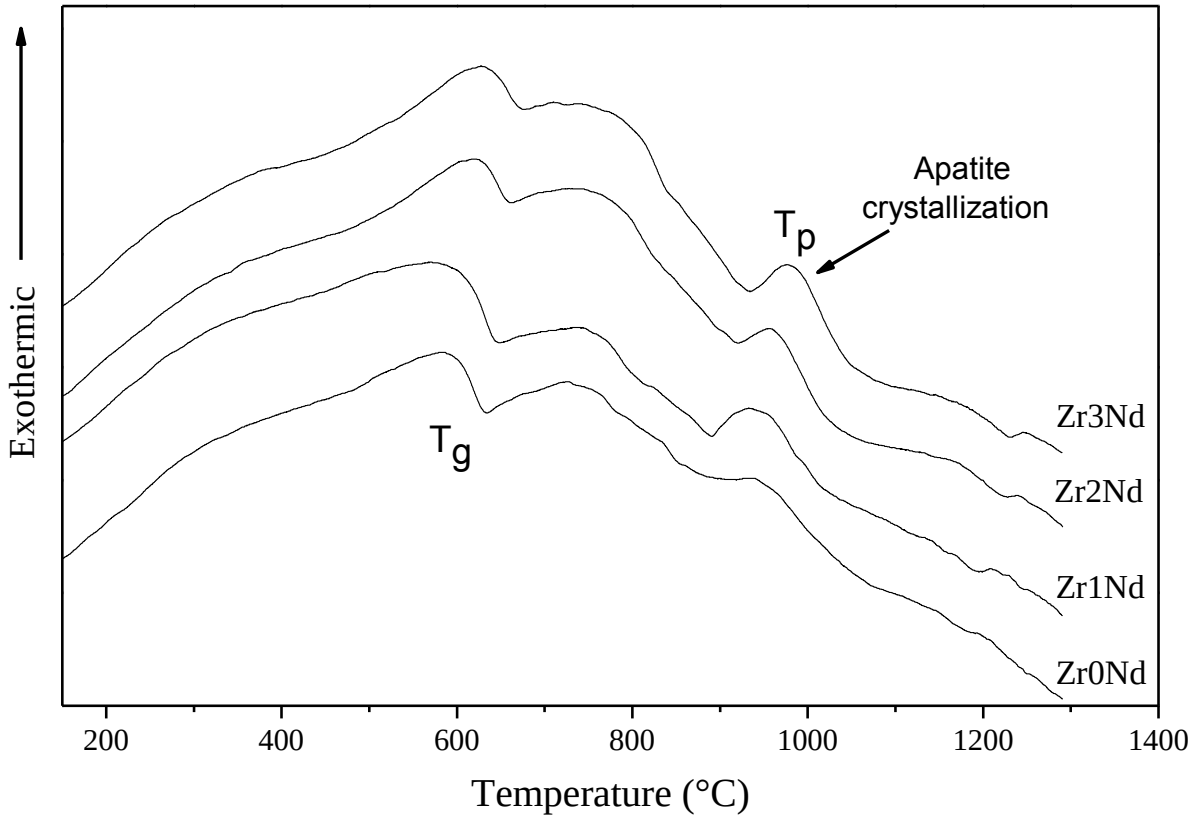
Exothermic
Apatite
crystallization
Tp
Tg
Zr3Nd
Zr2Nd
Zr1Nd
Zr0Nd
200
400
600
800
1000
1200
1400
Temperature (°C)

Figure 6

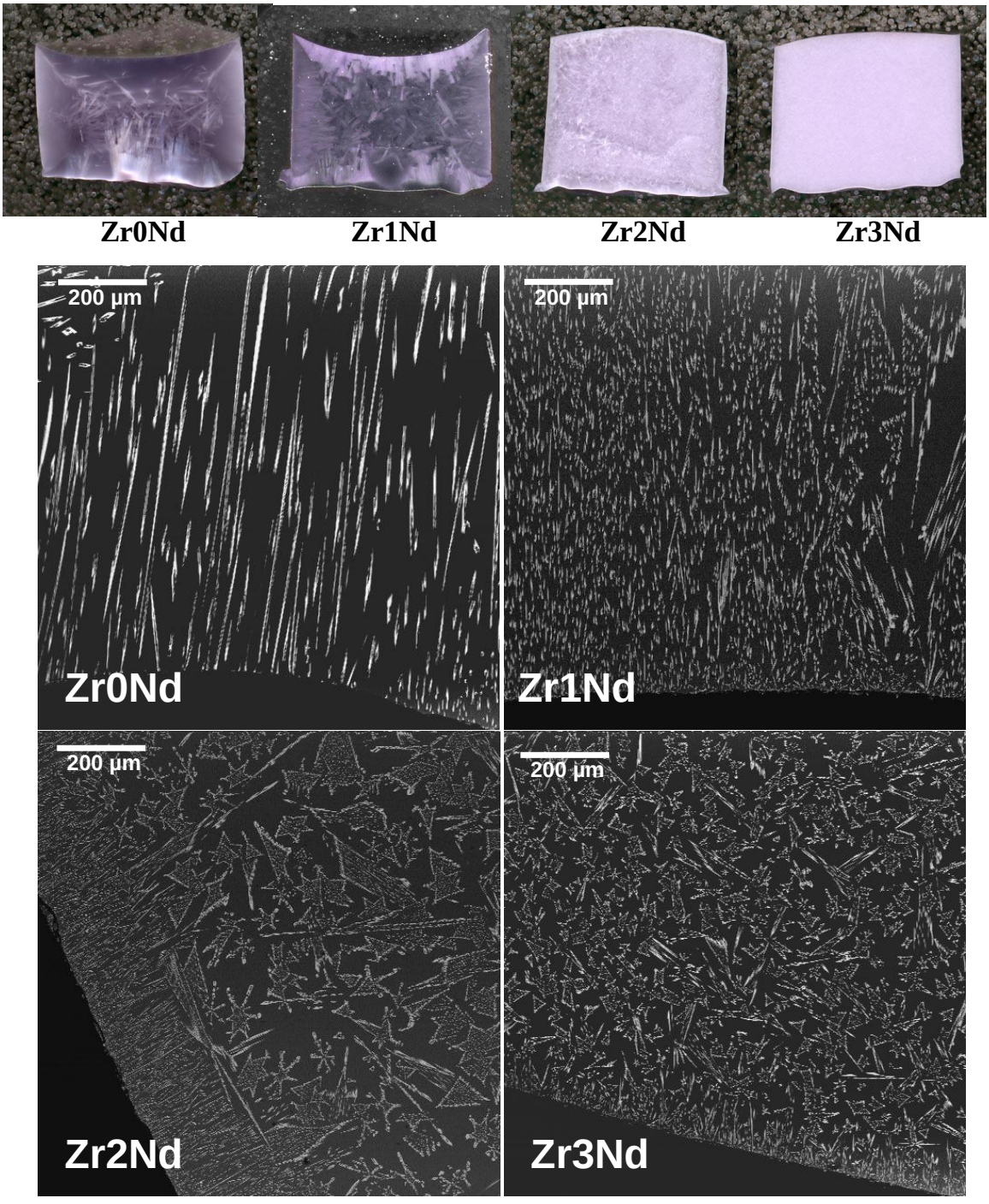
Zr0Nd
Zr1Nd
Zr2Nd
Zr3Nd
200 µm
Zr0Nd
200 µm
Zr1Nd
200 µm
Zr2Nd
200 µm
Zr3Nd

Figure 7

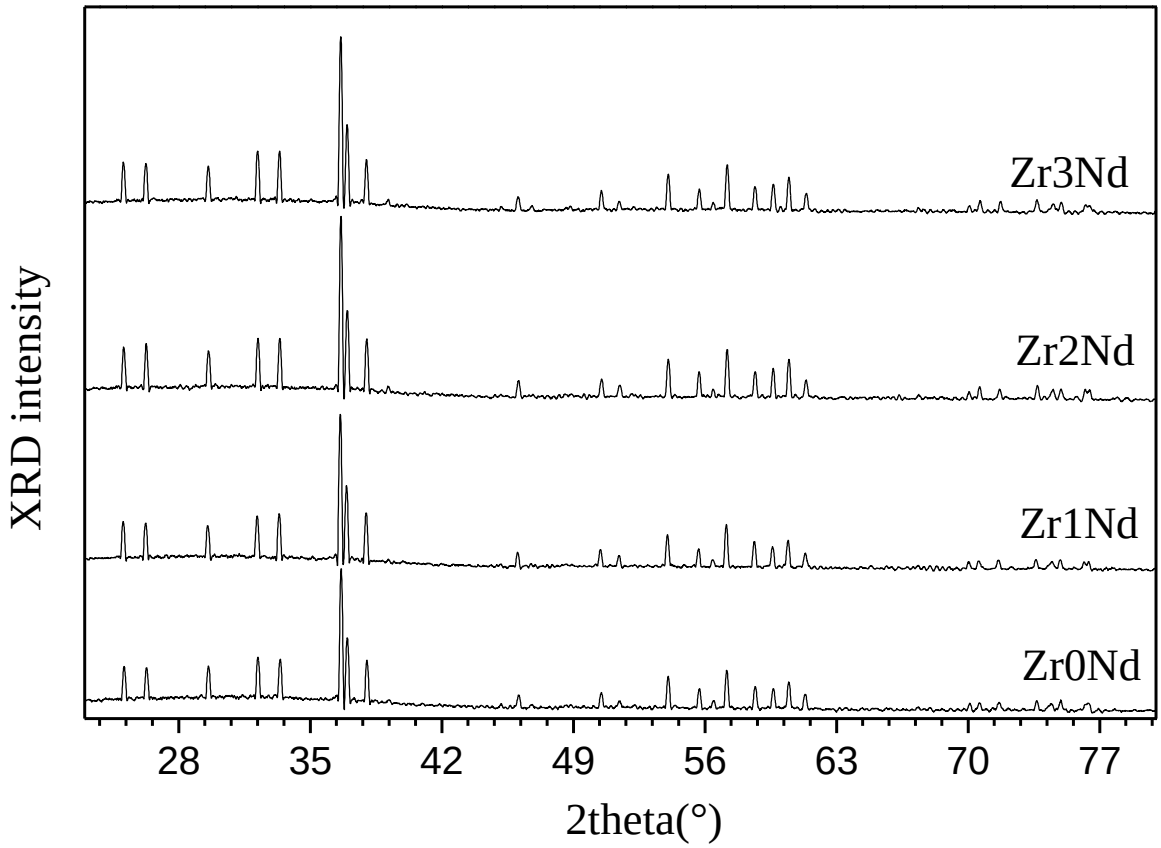
XRD intensity
Zr3Nd
Zr2Nd
Zr1Nd
Zr0Nd
28
35
42
49
56
63
70
77
2theta(°)

Figure 8

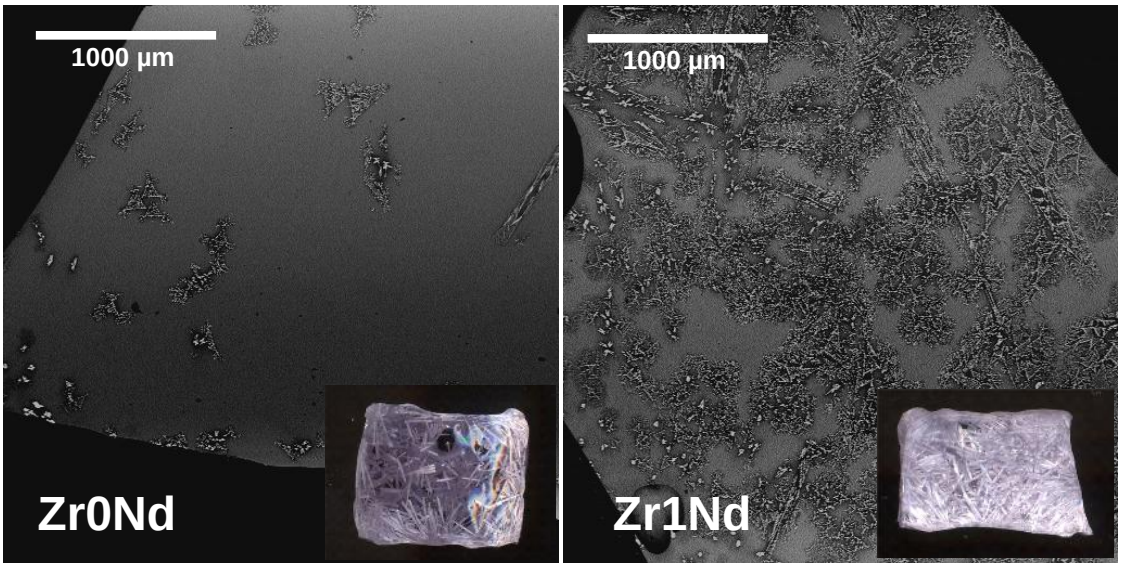

Figure 9

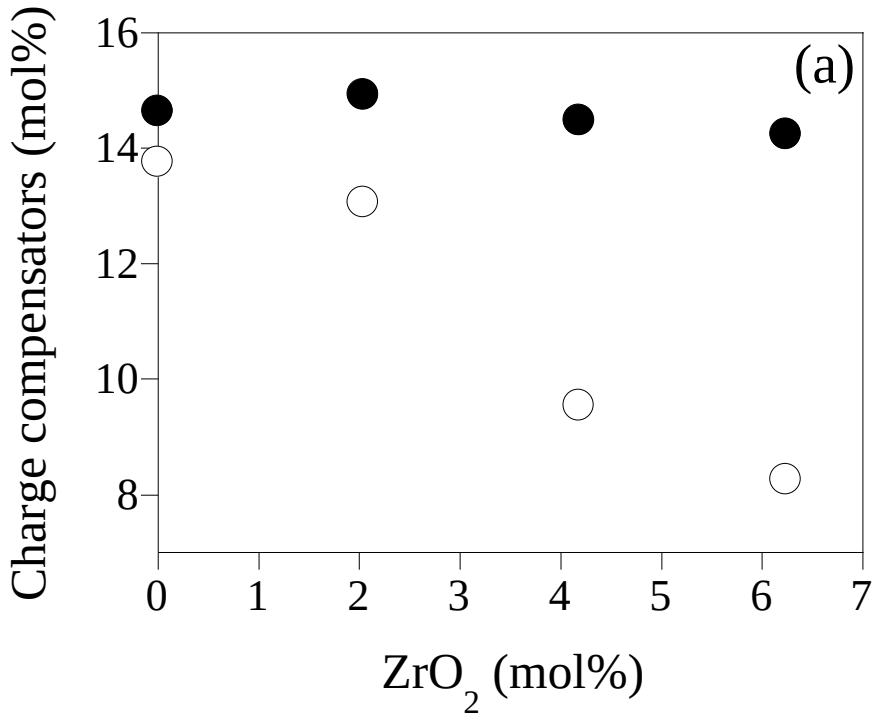
(a)
Charge compensators (mol%)
16
14
12
10
8
0
1
2
3
4
5
6
7
ZrO2 (mol%)

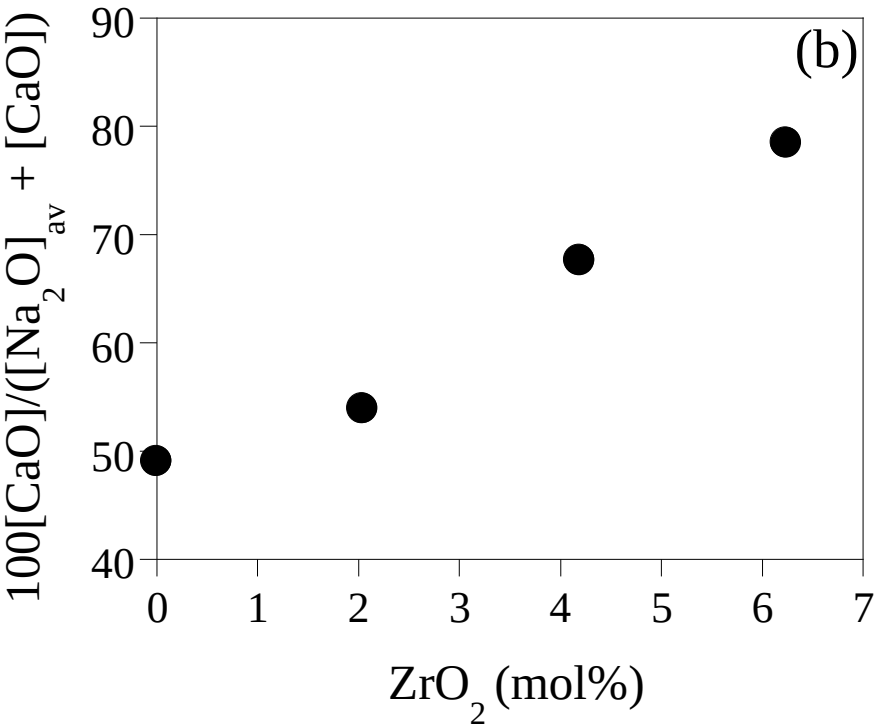
(b)
100[CaO]/([Na2O]av + [CaO])
90
80
70
60
50
40
0
1
2
3
4
5
6
7
ZrO2 (mol%)

References

[1] V. T. Ylmaz, E. E. Lachowski, F. P. Glasser, Chemical and microstructural changes at alkali-resistant glass fiber–cement interfaces, J. Amer. Ceram. Soc. 74 (1991) 3054-3060.

[2] G. H. Beall, R. L. Pinckney, Nanophase glass-ceramics, J. Amer. Ceram. Soc. 82 (1999) 5-16.

[3] W. Höland, V. Rheinberger, M. Schweiger, Control of nucleation in glass ceramics, Phil. Trans. R. Soc. Lond. A 361 (2003) 575-589.

[4] D.P. Mukherjee, S. Kumar Das, Role of ZrO_2 on properties of machinable glass-ceramics, Adv. Sci. Lett. 22 (2016) 202-207.

[5] D. Caurant, P. Loiseau, O. Majérus, V. Aubin-Chevaldonnet, I. Bardez, A. Quintas, Glasses, Glass-Ceramics and Ceramics for Immobilization of Highly Radioactive Nuclear Wastes, Nova Science Publishers, Hauppauge NY (2009).

[6] F. Angeli, T. Charpentier, M. Gaillard, P. Jollivet, Influence of zirconium of pristine and and leached soda-lime borosilicate glasses: Towards a quantitative approach by ^{17}O MQMAS NMR, J. Non-Cryst. Solids 354 (2008) 3713-3722.

[7] E. Pèlegrin, G. Calas, P. Ildefonse, P. Jollivet, L. Galoisy, Structural evolution of glass surface during alteration: Application to nuclear waste glasses, J. Non-Cryst. Solids 356, (2010) 2497-2508.

[8] R. A. Day, J. Ferenczy, E. Drabarek, T. Advocat, C. Fillet, J. Lacombe, C. Ladirat, C. Veyer, R. Do Quang, J. Thomasson, Glass-ceramics in a cold-crucible melter: the optimum combination for greater waste processing efficiency, WM'03 conference (Waste Management), February 23-27, 2003, Tucson, AZ Conference, http://www.wmsym.org/archives/2003/pdfs/249.pdf.

[9] A. J. Conelly, N. C. Hyatt, K. P. Travis, R. J. Hand, E. R. Madrell, R.J.Short, The structural role of Zr within alkali borosilicate glasses for nuclear waste immobilisation, J. Non-Cryst. Solids 357 (2011) 1647-1656.

[10] D. A. McKeown, I. S. Muller, A. C. Buechele, I. L. Pegg, C.A. Kendziora, Structural characterization of high-zirconia borosilicate glasses using Raman spectroscopy, J. Non-Cryst. Solids 262 (2000) 126-134.

[11] D. A. McKeown, I. S. Muller, A. C. Buechele, I. L. Pegg, X-ray absorption studies of the local environment of Zr in high-zirconia borosilicate glasses, J. Non-Cryst. Solids 258 (1999) 98-109.

[12] T. Plaisted, P. Hrma, J. Vienna, A. Jiricka, Liquidus temperature and primary crystallization phases in high-zirconia high-level waste borosilicate glasses, MRS proceedings 608 (1999) 709 -714.

[13] D. A. McKeown, I. S. Muller, A. C. Buechele, I. L. Pegg, C. A. Kendziora, C. R. Scales, formulation, testing, and structural characterization of high-zirconium high-level waste glasses, MRS proceedings 556 (1999) 305-312.

[14] O. Dargaud, L. Cormier, N. Menguy, L. Galoisy, G. Calas, S. Papin, G. Querel, L. Olivi, Structural role of Zr^{4+} as a nucleating agent in a $MgO–Al_2O_3–SiO_2$ glass-ceramics: A combined XAS and HRTEM approach, J. Non-Cryst. Solids 356 (2010) 2928-2934.

[15] L. Cormier, O. Dargaud, G. Calas, C. Jousseaume, S. Papin, N. Trcera, A. Cognigni, Zr environment and nucleation role in aluminosilicate glasses, Mater. Chem. Phys. 152 (2015) 41-47.

[16] M. Chavoutier, D. Caurant , O. Majérus, R. Boulesteix, P. Loiseau, C. Jousseaume, E. Brunet, E. Lecomte, Effect of TiO_2 content on the crystallization and the color of $(ZrO_2\text{-}TiO_2)$-doped $Li_2O\text{-}Al_2O_3\text{-}SiO_2$ glasses, J. Non Cryst. Solids 384 (2014) 15-24.

[17] A. Quintas, D. Caurant, O. Majérus, J. L. Dussossoy, T. Charpentier, Effect of changing the rare earth cation type on the structure and crystallization behavior of an aluminoborosilicate glass, Phys. Chem. Glasses: Eur. J. Glass Sci. Technol. B 49 (2008) 192-197.

[18] I. Bardez, D. Caurant, J.L. Dussossoy, P. Loiseau, C. Gervais, F. Ribot, D.R. Neuville, N. Baffier, C. Fillet, Matrices envisaged for the immobilization of concentrated nuclear waste solutions, Nucl. Sci. Eng. 153 (2006) 272-284.

[19] A. Quintas, D. Caurant, O. Majérus, P. Loiseau, T. Charpentier, J-L. Dussossoy, ZrO_2 addition in soda-lime aluminoborosilicate glasses containing rare earths: Impact on the network structure, J. Alloys Compd. 714 (2017) 47-62.

[20] D. Caurant, A. Quintas, O. Majérus, P. Loiseau, T. Charpentier, P. Vermaut, J-L. Dussossoy**,** Structural and crystallization study of a simplified aluminoborosilicate nuclear glass containing rare-earths: effect of ZrO_2 concentration, Mat. Res. Soc. Symp. Proc. 1265 (2010) 89-94.

[21] P. F. James, Nucleation in glass-forming systems - a review in: Nucleation and crystallization in glasses. Advances in ceramics vol. 4. J. H. Simmons, D.R. Uhlmann, G. H. Beall (Eds), The American Ceramic Society, Columbus, OH, (1982) 1-48.

[22] O. Majérus, D. Caurant, A. Quintas, J.L. Dussossoy, I. Bardez, P. Loiseau, Effect of boron oxide addition on the Nd^{3+} environment in a Nd-rich soda-lime aluminoborosilicate glass, J. Non-Cryst. Solids 357 (2011) 2744-2751.

[23] A. Quintas, O. Majérus, M. Lenoir, D. Caurant, K. Klementiev, A. Webb, Effect of alkali and alkaline-earth cations on the neodymium environment in a rare-earth rich aluminoborosilicate glass, J. Non-Cryst. Solids 354 (2008) 98-104.

[24] K. Gatterer, G. Pucker, W. Jantscher, H. P. Fritzer, S. Arafa, Suitability of Nd(III) absorption spectroscopy to probe the structure of glasses from the ternary system Na_2O–B_2O_3–SiO_2, J. Non-Cryst. Solids 231 (1998) 189-199.

[25] A. A. Dymnikov, A. K. Przhevuskii, Classification of Stark structure in spectra of Nd-doped glasses, J. Non-Cryst. Solids, 215 (1997) 83-95.

[26] T. Schaller, J. F. Stebbins, M. C. Wilding, Cation clustering and formation of free oxide ions in sodium and potassium lanthanum silicate glasses: nuclear magnetic resonance and Raman spectroscopic findings, J. Non-Cryst. Solids 243 (1999) 146-157.

[27] A. Bonamartini Corradi, V. Cannillo, M. Montorsi, C. Siligardi, A.N. Cormack, Structural characterization of neodymium containing glasses by molecular dynamics simulation, J. Non-Cryst. Solids 351 (2005) 1185-1191.

[28] A. Bonamartini Corradi, V. Cannillo, M. Monia, C. Siligardi, Local and medium range structure of erbium containing glasses: A molecular dynamics study, J. Non-Cryst. Solids 354 (2008) 173-180.

[29] A. Bonamartini Corradi, V. Cannillo, M. Montorsi, C. Siligardi, Influence of Al_2O_3 addition on thermal and structural properties of erbium doped glasses, J. Mater. Sci. 41 (2006) 2811-2819.

[30] J. Du, A. N. Cormack, The structure of erbium doped sodium silicate glasses, J. Non-Cryst. Solids 351 (2005) 2263-2276.

[31] B. Park, H. Li, L. R. Corrales, Molecular dynamics simulation of La_2O_3–Na_2O–SiO_2 glasses. I. The structural role of La^{3+} cations, J. Non-Cryst. Solids 297 (2002) 220-238.

[32] N. Chouard, D. Caurant, O. Majérus, J.-L. Dussossoy, A. Ledieu, S. Peuget, R. Baddour-Hadjean, J-P. Pereira-Ramos, Effect of neodymium oxide on the solubility of MoO_3 in an aluminoborosilicate glass, J. Non-Cryst. Solids 357 (2011) 2752-2762.

[33] O. Dargaud, G. Calas, L. Cormier, L. Galoisy, C. Jousseaume, G. Querel, M. Newville, In situ study of nucleation of zirconia in an $MgO–Al_2O_3–SiO_2$ glass, J. Amer. Ceram. Soc. 93 (2010) 342-344.

[34] O. Dargaud, L. Cormier, N. Menguy, G. Patriarche, G. Calas, Mesoscopic scale description of nucleation processes in glasses, Appl. Phys. Lett. 99 (2011) 021904.

[35] L. Cormier, B. Cochain, A. Dugué, O. Dargaud, Transition elements and nucleation in glasses using X-ray absorption spectroscopy, Int. J. Appl. Glass Sci. 5 (2014) 126-135.

[36] O. Dargaud, L. Cormier, N. Menguy, G. Patriarche, Multi-scale structuration of glasses: Observations of phase separation and nanoscale heterogeneities in glasses by Z-contrast scanning electron transmission microscopy, J. Non-Cryst. Solids 358 (2012) 1257-1262.

[37] A. Quintas, O. Majérus, D. Caurant, J.L. Dussossoy, P. Vermaut, Crystallization of a rare earth-rich aluminoborosilicate glass with varying CaO/Na_2O ratio, J. Am. Ceram. Soc. 90 (2007) 712-719.

[38] D. Caurant, Spectroscopic investigations on glasses, glass-ceramics and ceramics developed for nuclear waste immobilization, Opt. Spectrosc. 116 (2014) 667–676.

[39] A. Kidari, J-L. Dussossoy, E. Brackx, D. Caurant, M. Magnin, I. Bardez-Giboire, Lanthanum and neodymium solubility in simplified $SiO_2–B_2O_3–Na_2O–Al_2O_3–CaO$ high level waste glass, J. Am. Ceram. Soc. 95 (2012) 2537-2544.

[40] N. Chouard, D. Caurant, O. Majérus, J-L. Dussossoy, S. Klimin, D. Pytalev, R. Baddour-Hadjean, J-P. Pereira-Ramos, Effect of MoO_3, Nd_2O_3 and RuO_2 on the crystallization of soda-lime aluminoborosilicate glasses, J. Mater. Sci. 50 (2015) 219-241.

[41] W. J. Weber, F. P. Roberts, A review of radiation effects in solid nuclear waste forms, Nucl. Technol. 60 (1983) 178-197.

[42] D. Caurant, O. Majérus, P. Loiseau, I. Bardez, N. Baffier, J.L. Dussossoy, Crystallization of neodymium-rich phases in silicate glasses developed for nuclear waste immobilization, J. Nucl. Mater. 354 (2006) 143-162.

[43] D. Zhao, L. Li, L.L. Davis, W.J. Weber, R.C. Ewing, Gadolinium borosilicate glass-bonded Gd-silicate apatite: a glass-ceramic nuclear waste form for actinides, Mater. Res. Soc. Symp. Proc. 663 (2001) 199.